

Exponential Stability and Design of Sensor Feedback Amplifiers for Fast Stabilization of Magnetizable Piezoelectric Beam Equations

Ahmet Özkan Özer¹, *Member, IEEE*, Ahmet Kaan Aydın² *Member, IEEE*, and Rafi Emran³

Abstract—The dynamic partial differential equation (PDE) model governing longitudinal oscillations in magnetizable piezoelectric beams exhibits exponentially stable solutions when subjected to two boundary state feedback controllers. An analytically established exponential decay rate by the Lyapunov approach ensures stabilization of the system to equilibrium, though the actual decay rate could potentially be improved. The decay rate of the closed-loop system is highly sensitive to the choice of material parameters and the design of the state feedback amplifiers. This paper focuses on investigating the design of state feedback amplifiers to achieve a maximal exponential decay rate, which is essential for effectively suppressing oscillations in these beams. Through this design process, we explicitly determine the safe intervals of feedback amplifiers that ensure the theoretically found maximal decay rate, with the potential for even better rates. Our numerical results reaffirm the robustness of the decay rate within the chosen range of feedback amplifiers, while deviations from this range significantly impact the decay rate. To underscore the validity of our results, we present various numerical experiments.

Index Terms—Intelligent Materials, Distributed Parameter Systems, Feedback Stabilization, Maximal Decay Rate, Lyapunov Approach

I. INTRODUCTION

Piezoelectric ceramics, including lead-free materials like barium titanate, sodium potassium niobate, and sodium bismuth titanate, are renowned multifunctional smart materials that generate electric displacement in response to mechanical stress [26]. Their small size and high power density make them ideal for various industrial applications, including implantable biomedical devices [5], [25], wearable interfaces with PVDF sensors [7], biocompatible sensors [32], and ultrasound imagers and cleaners [24]. Their fast response, large mechanical force, and fine resolution contribute to their effectiveness [10].

Consider a piezoelectric beam, clamped on one side and free on the other, with sensors for tip velocity and current. The beam is of length L and thickness h . Assume that the transverse oscillations of the beam are negligible, so the longitudinal vibrations, in the form of expansion and compression

of the center line of the beam, are the only oscillations of note together with the electromagnetic effects. Existing mathematical models often oversimplify intrinsic mechanical or electromagnetic interactions, impacting boundary feedback stabilizability [1], [6], [17], [20], [27], [29].

While electrostatic and quasi-static approaches based on Maxwell's equations are typically sufficient for non-magnetizable piezoelectric beams, assessing radiated electromagnetic power requires consideration of electromagnetic waves generated by mechanical fields [28]. Therefore, fully dynamic models of piezoelectric beams are essential. Denoting $v(x, t)$ as the longitudinal oscillations and $p(x, t)$ as the total charge accumulated at the electrodes, the equations of motion form following system of partial differential equations [17]

$$\begin{aligned} \begin{bmatrix} \rho & 0 \\ 0 & \mu \end{bmatrix} \begin{bmatrix} v_{tt} \\ p_{tt} \end{bmatrix} - \begin{bmatrix} \alpha & -\gamma\beta \\ -\gamma\beta & \beta \end{bmatrix} \begin{bmatrix} v_{xx} \\ p_{xx} \end{bmatrix} &= \begin{bmatrix} 0 \\ 0 \end{bmatrix}, \\ (v, p)(0, t) &= 0, \\ \begin{bmatrix} \alpha & -\gamma\beta \\ -\gamma\beta & \beta \end{bmatrix} \begin{bmatrix} v_x \\ p_x \end{bmatrix} (L, t) &= \begin{bmatrix} u_1(t) \\ u_2(t) \end{bmatrix}, \quad t \in \mathbb{R}^+ \\ [v, p, v_t, p_t](x, 0) &= [v_0, p_0, v_1, p_1](x), \quad x \in [0, L] \end{aligned} \quad (1)$$

where ρ , α , β , γ , and μ are the mass density per unit volume, the elastic stiffness, the impermeability, the piezoelectric constant, and the magnetic permeability, respectively, and $u_1(t)$ and $u_2(t)$ are strain and voltage actuators, respectively.

Define $\alpha := \alpha_1 + \gamma^2\beta > 0$ with $\alpha_1 > 0$, and

$$\zeta^\mp = \frac{1}{\sqrt{2}} \sqrt{\frac{\alpha\mu}{\alpha_1\beta} + \frac{\rho}{\alpha_1}} \mp \sqrt{\left(\frac{\alpha\mu}{\alpha_1\beta} + \frac{\rho}{\alpha_1}\right)^2 - \frac{4\rho\mu}{\beta\alpha_1}}. \quad (2)$$

Note that $\sqrt{\frac{\rho}{\alpha}}$ and $\sqrt{\frac{\beta}{\mu}}$ are non-identical and represent significantly different wave propagation speeds in (1). The natural energy of the solutions is defined as

$$\begin{aligned} E(t) = \frac{1}{2} \int_0^L \left[\rho |v_t|^2 + \mu |p_t|^2 + \alpha_1 |v_x|^2 \right. \\ \left. + \beta |\gamma v_x - p_x|^2 \right] dx. \end{aligned} \quad (3)$$

The exact observability result for the model (1) with $u_1(t)$, $u_2(t) = 0$ and with only one sensor measurement is not possible [17]. However, by employing two sensor measurements, $v_t(L, t)$ (tip velocity) and $p_t(L, t)$ (total current accumulated at electrodes), a suboptimal observation time is achieved [23]. This result is later refined to include the optimal observation time [21].

¹Department of Mathematics, Western Kentucky University, Bowling Green, KY 42101, USA. ozkan.ozer@wku.edu

²Department of Mathematics, University of Maryland, Baltimore County, Baltimore, MD 21250, USA. aaydin1@umbc.edu

³Department of Mathematical Sciences, New Jersey Institute of Technology, Newark, NJ 07102, USA. ms3532@njit.edu

Theorem 1: [21, Theorem 2.2] Define the Hilbert spaces $(H_*^1(0, L)) = \{z \in H^1(0, L) : z(0) = 0\}$ and $\mathcal{H} = (H_*^1(0, L))^2 \times (L^2(0, L))^2$. For all initial data $[v_0, p_0, v_1, p_1](x) \in \mathcal{H}$, and for any $T > \frac{2L}{\max\{\zeta^-, \zeta^+\}}$, there exists a constant $C(T) > 0$ such that the weak solutions $(v, p, v_t, p_t) \in \mathcal{H}$ of the control-free system (1), i.e., $u_1(t), u_2(t) = 0$, satisfy

$$\int_0^T \left(\rho |v_t(L, t)|^2 + \mu |p_t(L, t)|^2 \right) dt \geq C(T)E(0). \quad (4)$$

When the observed sensor signals $v_t(L, t)$ and $p_t(L, t)$ are amplified and fed back to (1), a closed-loop system is formed. The amplification range depends on the sensor limits. While using only one sensor feedback can make the system energy dissipative, it is insufficient for exponential stabilization in \mathcal{H} . This is because the closed-loop system with this control design imposes strict conditions on stabilization results [17]. Exponential stability is jeopardized for a large class of material parameters and is only achievable for a small subset [18].

Let $\xi_1, \xi_2 > 0$ be the feedback amplifiers for the two sensor measurements of the closed-loop system $v_t(L, t)$ and $p_t(L, t)$, respectively. The strain and voltage actuators $u_1(t)$ and $u_2(t)$ are chosen to be proportional to the sensor feedback amplifiers,

$$\begin{bmatrix} u_1(t) \\ u_2(t) \end{bmatrix} = - \begin{bmatrix} \xi_1 & 0 \\ 0 & \xi_2 \end{bmatrix} \begin{bmatrix} \dot{v}(L, t) \\ \dot{p}(L, t) \end{bmatrix}. \quad (5)$$

The exponential stability of the closed-loop system (1), (5) has been studied in [23], where the proof relies on decomposing the system into conservative and dissipative components. However, this method does not explicitly describe the decay rate or allow optimization of the feedback amplifiers.

The primary objective of this paper is to establish the existence of an exponential decay rate for the system described by (1) and (5) through the meticulous construction of a Lyapunov function. Given the impracticality of traditional spectral analysis due to the strong coupling in the wave system, we adopt a multiplier approach combined with an optimization argument to define a safe range of intervals for each feedback amplifier ξ_1 and ξ_2 . This ensures that the decay rate provided by the Lyapunov approach is achievable for any type of initial conditions \mathcal{H} .

Our methodology provides a maximal decay rate for the system, serving as an upper bound to the optimal decay rate since the actual decay rate could potentially be even better. Existing literature on optimal actuator designs commonly offers different approaches for infinite-dimensional systems [8], [13], [15], [22], and finite-dimensional systems [4], [9]. Our approach is particularly valuable for model reductions by Finite Differences or Finite Elements [21] for (1). Notably, the Lyapunov-based exponential stability proof [2], uniformly as the discretization parameter $h \rightarrow 0$ with the recently proposed order-reduced Finite Differences [12], closely resembles the approach employed here.

II. EXPONENTIAL STABILITY RESULT

For the solutions of the system (1),(5) to stabilize exponentially, the energy must be dissipative. The proof of the following dissipativity theorem is omitted.

Lemma 1: For all $t > 0$, the energy $E(t)$ in (3) is dissipative. In other words,

$$\frac{dE}{dt} = -\xi_1 |\dot{v}(L, t)|^2 - \xi_2 |\dot{p}(L, t)|^2 \leq 0.$$

Now, let's define an energy-like functional $F(t)$ in order to establish a perturbed energy functional $E_\delta(t)$ as follows

$$F(t) := \int_0^L (\rho v_t x v_x + \mu p_t x p_x) dx, \quad (6)$$

$$E_\delta(t) := E(t) + \delta F(t). \quad (7)$$

Here, $\delta > 0$ will be determined as a function of sensor feedback amplifiers ξ_1 and ξ_2 later.

The following two lemmas for $F(t)$ and $E_\delta(t)$ are needed to prove our main exponential stability result. Let

$$\eta := \max \left(\sqrt{\frac{\rho}{\alpha_1}} + \sqrt{\frac{\mu\gamma^2}{\alpha_1}}, \sqrt{\frac{\mu}{\beta}} + \sqrt{\frac{\mu\gamma^2}{\alpha_1}} \right), \quad (8)$$

Lemma 2: Letting $0 < \delta < \frac{1}{\eta L}$, for all $t > 0$, $E_\delta(t)$ in (7) is equivalent to $E(t)$ in (3). In other words,

$$(1 - \delta\eta L) E(t) \leq E_\delta(t) \leq (1 + \delta\eta L) E(t). \quad (9)$$

Proof: By the Hölder's, Minkowski's, Triangle inequalities, as well as algebraic manipulations, $F(t)$ satisfies

$$\begin{aligned} |F(t)| &\leq L \left[\left(\int_0^L \rho |v_t|^2 dx \right)^{\frac{1}{2}} \left(\frac{\rho}{\alpha_1} \int_0^L \alpha_1 |v_x|^2 dx \right)^{\frac{1}{2}} \right. \\ &\quad \left. + \left(\int_0^L \mu |p_t|^2 dx \right)^{\frac{1}{2}} \left\{ \left(\int_0^L \mu |\gamma v_x - p_x|^2 dx \right)^{\frac{1}{2}} \right. \right. \\ &\quad \left. \left. + \left(\mu \int_0^L \gamma^2 |v_x|^2 dx \right)^{\frac{1}{2}} \right\} \right] \\ &\leq \frac{L}{2} \left[\sqrt{\frac{\rho}{\alpha_1}} \int_0^L \rho |v_t|^2 dx + \left(\sqrt{\frac{\rho}{\alpha_1}} + \sqrt{\frac{\mu\gamma^2}{\alpha_1}} \right) \int_0^L \alpha_1 |v_x|^2 dx \right. \\ &\quad \left. + \left(\sqrt{\frac{\mu}{\beta}} + \sqrt{\frac{\mu\gamma^2}{\alpha_1}} \right) \int_0^L \mu |p_t|^2 dx + \sqrt{\frac{\mu}{\beta}} \int_0^L \beta |\gamma v_x - p_x|^2 dx \right] \\ &\leq L\eta E(t). \end{aligned}$$

Since $|F(t)| \leq L\eta E(t)$, this leads to $|E_\delta(t)| \leq |E(t)| + \delta |F(t)| \leq (1 + L\eta\delta) E(t)$, and analogously, $|E_\delta(t)| \geq (1 - L\eta\delta) E(t)$, and therefore, (9) is immediate ■

Lemma 3: For any $\epsilon, t > 0$, $F(t)$ in (6) satisfies the following inequalities,

$$\begin{aligned} \frac{dF}{dt} &\leq -E(t) + \frac{L}{2} \left[\rho + \frac{(1+\epsilon)\xi_1^2}{\alpha_1} \right] |v_t(L, t)|^2 \\ &\quad + \frac{L}{2} \left[\mu + \left(1 + \frac{1}{\epsilon}\right) \frac{\xi_2^2 \gamma^2}{\alpha_1} + \frac{\xi_2^2}{\beta} \right] |p_t(L, t)|^2. \end{aligned} \quad (10)$$

Proof: Recalling $\alpha_1 = \alpha - \gamma^2\beta$, and (1),

$$\begin{aligned} \frac{dF}{dt} &= \frac{L}{2} \beta (\gamma v_x(L, t) - p_x(L, t))^2 + \frac{L}{2} \alpha_1 (v_x(L, t))^2 \\ &\quad + \frac{L}{2} \left[\rho |v_t(L, t)|^2 + \mu |p_t(L, t)|^2 \right] - E(t). \end{aligned}$$

Next, the boundary conditions are used so that

$$\begin{aligned} \frac{dF}{dt} &= -E(t) + \frac{L}{2} \left(\mu + \frac{\xi_2^2}{\beta} \right) |p_t(L, t)|^2 \\ &\quad + \frac{L\rho}{2} |v_t(L, t)|^2 + \frac{L}{2\alpha_1} (\xi_1 |v_t(L, t)| + \xi_2 \gamma |p_t(L, t)|)^2. \end{aligned}$$

Finally, by the generalized Young's inequality with ϵ (or Peter-Paul inequality), (10) is obtained for any $\epsilon > 0$. ■

Now, the exponential stability result takes the following form

Theorem 2: The energy $E(t)$ of solutions decays exponentially, i.e. for any $\epsilon > 0$,

$$\begin{aligned} E(t) &\leq ME(0)e^{-\sigma t}, & \forall t > 0 \\ \sigma(\delta) &= \delta(1 - \delta L\eta), & M(\delta) = \frac{1 + \delta L\eta}{1 - \delta L\eta}, \end{aligned} \quad (11)$$

$$\begin{cases} \delta(\xi_1, \xi_2, \epsilon) < \frac{1}{\eta} \min\left(\frac{1}{\eta}, f_1(\xi_1, \epsilon), f_2(\xi_2, \epsilon)\right), \\ f_1(\xi_1, \epsilon) := \frac{2\xi_1\alpha_1}{\rho\alpha_1 + (1+\epsilon)\xi_1^2}, \\ f_2(\xi_2, \epsilon) := \frac{2\xi_2\epsilon\alpha_1\beta}{\epsilon\mu\alpha_1\beta + (\epsilon\alpha + \gamma^2\beta)\xi_2^2}. \end{cases} \quad (12)$$

Proof: Considering $\frac{dE_\delta}{dt} = \frac{dE}{dt} + \delta\frac{dF}{dt}$ with Lemma 3

$$\begin{aligned} \frac{dE_\delta}{dt} &\leq \underbrace{\left[\frac{\delta L}{2} \left[\rho + \frac{(1+\epsilon)\xi_1^2}{\alpha_1}\right] - \xi_1\right]}_{\leq 0} |v_t(L, t)|^2 \\ &+ \underbrace{\left[\frac{\delta L}{2} \left[\mu + \frac{(\epsilon\alpha + \gamma^2\beta)\xi_2^2}{\epsilon\alpha_1\beta}\right] - \xi_2\right]}_{\leq 0} |p_t(L, t)|^2 - \delta E(t) \end{aligned}$$

where δ is chosen to make the coefficients nonpositive, i.e. $\delta < \frac{1}{L} \min\left(\frac{1}{\eta}, f_1(\xi_1, \epsilon), f_2(\xi_2, \epsilon)\right)$. Next, by the equivalence of $E(t)$ and $E_\delta(t)$ from Lemma 2,

$$\frac{dE_\delta}{dt} \leq -\delta(1 - \delta L\eta) E_\delta(t). \quad (13)$$

By choosing $\sigma = \delta(1 - \delta L\eta) > 0$, together with (13) lead to

$$E_\delta(t) \leq E_\delta(0)e^{-\sigma t}. \quad (14)$$

Hence, (14) with Lemma 2 lead to the desired result. ■

III. OPTIMIZATION OF SENSOR FEEDBACK AMPLIFIERS

The decay rate $-\sigma$ in Theorem 2 provides an upper bound for the exponential decay rate of the system. In this section, we provide an optimization process for feedback amplifiers ξ_1 and ξ_2 that ensure the maximal value of σ , given by

$$\sigma_{max}(\delta) = \frac{1}{4\eta L} \text{ achieved at } \delta = \frac{1}{2\eta L}. \quad (15)$$

Since δ and σ are functions of ϵ and the sensor feedback amplifiers ξ_1 and ξ_2 in (5), the following results provide intervals for the feedback amplifiers and ϵ that ensures the decay rate (15) is attained.

Theorem 3: Define non-negative constants

$$\begin{aligned} c_1^\pm &:= \frac{2\alpha_1\eta \pm \sqrt{4\alpha_1^2\eta^2 - (1+\epsilon)\rho\alpha_1}}{1+\epsilon}, \\ c_2^\pm &:= \frac{2\epsilon\alpha_1\beta\eta \pm \sqrt{4(\epsilon\alpha_1\beta\eta)^2 - (\epsilon\alpha + \beta\gamma^2)\epsilon\mu\alpha_1\beta}}{\epsilon\alpha + \beta\gamma^2}, \end{aligned} \quad (16)$$

with any ϵ such that

$$\frac{\beta\gamma^2\mu}{4\alpha_1\beta\eta^2 - \alpha\mu} < \epsilon < \frac{4\alpha_1\eta^2 - \rho}{\rho}. \quad (17)$$

The decay rate $-\sigma_{max}(\delta)$ is achieved for the closed-loop system (1),(5) when the feedback amplifiers are chosen such as $\xi_1 \in (c_1^-, c_1^+)$, $\xi_2 \in (c_2^-, c_2^+)$.

Proof: Observe that to achieve the $\sigma_{max}(\delta)$ in (15), it is sufficient to have $f_1(\xi_1, \epsilon) > \frac{1}{2\eta}$ and $f_2(\xi_2, \epsilon) > \frac{1}{2\eta}$.

Thus, $f_1(\xi_1, \epsilon) > \frac{1}{2\eta}$, i.e. $\frac{2\xi_1\alpha_1}{\rho\alpha_1 + (1+\epsilon)\xi_1^2} > \frac{1}{2\eta}$, implies that

$$\epsilon < h_1(\xi_1) := \frac{4\alpha_1\xi_1\eta - \rho\alpha_1 - \xi_1^2}{\xi_1^2}. \quad (18)$$

Noting that $4\alpha_1^2\eta^2 - \rho\alpha_1 > 0$ by (8), $h_1(\xi_1)$ defines an upper bound for ϵ , and observe that ξ_1 must be chosen in between the following roots of h_1 to ensure $\epsilon > 0$, see Fig. 1

$$a_1^\pm := 2\alpha_1\eta \pm \sqrt{4\alpha_1^2\eta^2 - \rho\alpha_1},$$

Observe that $h_1(\xi_1) \geq 0$ if and only if $\xi_1 \in (a_1^-, a_1^+)$. Seeking the critical points of $h_1(\xi_1)$, $\frac{\partial h_1}{\partial \xi_1} = \frac{-4\xi_1^2\alpha_1\eta + 2\xi_1\rho\alpha_1}{\xi_1^4} = 0$, leads to $\xi_1 = \frac{\rho}{2\eta}$, for which h_1 achieves its maximum value.

Substituting $h_1\left(\xi_1 = \frac{\rho}{2\eta}\right)$ into (18) yields the following upper bound for ϵ

$$\epsilon < \frac{4\alpha_1\eta^2 - \rho}{\rho}. \quad (19)$$

By $f_2(\xi_2, \epsilon) > \frac{1}{2\eta}$, $\epsilon > h_2(\xi_2) := \frac{\beta\gamma^2\xi_2^2}{4\alpha_1\beta\xi_2\eta - \mu\alpha_1\beta - \alpha\xi_2^2}$. Since $\epsilon > 0$, the denominator $4\alpha_1\beta\xi_2\eta - \mu\alpha_1\beta - \alpha\xi_2^2$ is chosen to be strictly positive. This leads to $\xi_2 \in (a_2^-, a_2^+)$ where

$$a_2^\pm := \frac{2\alpha_1\beta\eta \pm \sqrt{4\alpha_1^2\beta^2\eta^2 - \alpha\mu\alpha_1\beta}}{\alpha}, \quad (20)$$

and $\xi_2 = a_2^-$ and $\xi_2 = a_2^+$ are the two vertical asymptotes of $h_2(\xi_2)$, see dashed lines in Fig. 1. Note that this condition ensures $h_2(\xi_2) \geq 0$. Seeking the critical points of $h_2(\xi_2)$ leads to $\xi_2 = \frac{\mu}{\eta}$, for which $h_2(\xi_2)$ takes its minimum value.

Substituting $h_2\left(\frac{\mu}{\eta}\right)$ into (18) yields the lower bound for ϵ

$$\epsilon > \frac{\beta\gamma^2\mu}{4\alpha_1\beta\eta^2 - \alpha\mu} \quad (21)$$

where $4\alpha_1\beta\eta^2 - \alpha\mu > 0$ by (8). Restricting $h_1(\xi_1)$ and $h_2(\xi_2)$ in between roots and asymptotes, respectively, ϵ values corresponding to the filled regions in Fig. 1 satisfy conditions (19) and (21), respectively.

For any ϵ that satisfies (17), $f_1(\xi_1) > \frac{1}{2\eta}$, and $f_2 > \frac{1}{2\eta}$, i.e.

$$\begin{aligned} -(1+\epsilon)\xi_1^2 + 4\alpha_1\eta\xi_1 - \rho\alpha_1 &\geq 0, \\ -(\epsilon\alpha + \beta\gamma^2)\xi_2^2 + 4\epsilon\alpha_1\beta\eta\xi_2 - \epsilon\mu\alpha_1\beta &\geq 0, \end{aligned}$$

yield $\xi_1 \in (c_1^-, c_1^+)$ and $\xi_2 \in (c_2^-, c_2^+)$, respectively.

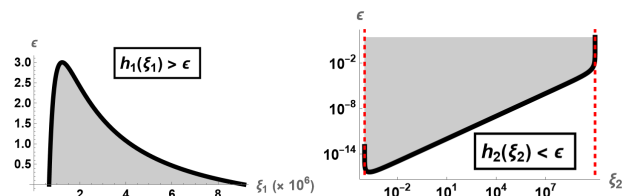


Fig. 1. For the material parameters in Table I, bounds of ϵ depend on $h_1(\xi_1)$ and $h_2(\xi_2)$. Note that the h_2 -plot is logarithmic.

We prove that such $\xi_1 \in (c_1^-, c_1^+)$ and $\xi_2 \in (c_2^-, c_2^+)$ exist. Note that the sufficient condition for $(c_1^-, c_1^+), (c_2^-, c_2^+) \neq \emptyset$ is the existence of ϵ satisfying (17) which is ensured by

$$\frac{4\alpha_1\eta^2 - \rho}{\rho} \geq \frac{3\alpha_1\eta^2}{\rho} \geq 3, \quad \frac{\beta\gamma^2\mu}{4\alpha_1\beta\eta^2 - \alpha\mu} \leq \frac{\beta\gamma^2\mu}{3\alpha\mu} \leq \frac{1}{3}. \quad (22)$$

The amplifier ξ_1 maximizing h_1 and the amplifier ξ_2 minimizing h_2 are always in the respective intervals, i.e. $\xi_1 = \frac{\rho}{2\eta} \in (c_1^-, c_1^+)$ and $\xi_2 = \frac{\mu}{\eta} \in (c_2^-, c_2^+)$. Moreover, as ϵ approaches to the upper (lower) bound (c_1^-, c_1^+) gets smaller (larger) and (c_2^-, c_2^+) gets larger (smaller), see Fig. 2. Feedback amplifiers chosen within the intervals ensure that $f_1(\xi_1) \geq \frac{1}{2\eta}$ and $f_2(\xi_2) \geq \frac{1}{2\eta}$ are satisfied, see Figs. 3 and 4. ■

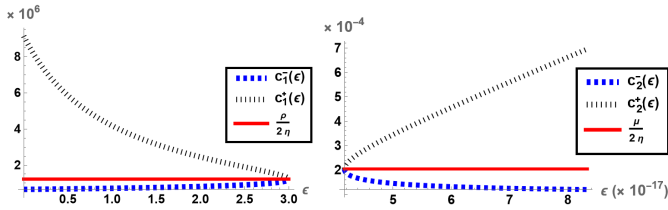


Fig. 2. For the material parameters in Table I, graphs of c_1^\pm , c_2^\pm with respect to ϵ satisfy the inequalities in (17).

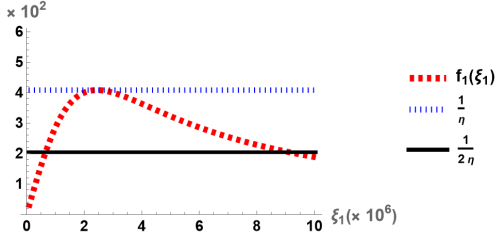


Fig. 3. For $\epsilon \approx 10^{-15}$, $f_1(\xi_1) > \frac{1}{2\eta}$ when $\xi_1 \in (c_1^-, c_1^+)$.

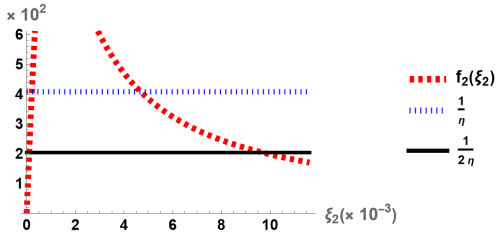


Fig. 4. For $\epsilon \approx 10^{-15}$, $f_2(\xi_2) > \frac{1}{2\eta}$ when $\xi_2 \in (c_2^-, c_2^+)$.

IV. SIMULATIONS AND NUMERICAL EXPERIMENTS

In this section, we present numerical simulations primarily aimed at demonstrating the following:

- The exponential stability of the system (1) with (5) is showcased using feedback amplifiers $\xi_1 \in (c_1^-, c_1^+)$ and $\xi_2 \in (c_2^-, c_2^+)$, as obtained in Theorem 3.
- Comparison of the reduced model exponential decay rates for a selection of feedback amplifiers.

Moreover, we address a common challenge encountered in standard model reductions, such as Finite Differences (FD) and Finite Elements (FE), which introduce spurious high-frequency vibrational modes to the system. These spurious modes significantly impact the decay rate of the system. In fact, reduced models lack the uniform observability property as the mesh parameter approaches zero, necessitating filtering techniques such as the direct Fourier filtering [3], [11] or the indirect filtering [30].

To mitigate the adverse effects of approximation methods on the decay rate, we consider a recently introduced technique known as Order-Reduced Finite Differences (ORFD) [12]. The ORFD method has been observed to retain the decay rate of the infinite-dimensional system. For rigorous stability analyses of all three approximations, interested readers can refer to [2].

Consider a given natural number $N \in \mathbb{N}$, which denotes the number of nodes in the spatial semi-discretization. Let's introduce the mesh size as $h := \frac{1}{N+1}$, and discretize the

interval $[0, L]$ as $0 = x_0 < x_1 < \dots < x_j = j \cdot h < \dots < x_N < x_{N+1} = L$. Let $(v_j, p_j) = (v_j, p_j)(t) \approx (v, p)(x_j, t)$ be the approximation of the solution $(v, p)(x, t)$ of (1)-(5) at the point space $x_j = j \cdot h$ for any $j = 0, 1, \dots, N, N+1$, and let $\vec{v} = [v_1, v_2, \dots, v_{N+1}]^T$ and $\vec{p} = [p_1, p_2, \dots, p_{N+1}]^T$.

In the ORFD method, in addition to the standard nodes $\{x_j\}_{j=0}^N$, we also consider the in-between middle nodes of each subinterval, denoted by $\left\{x_{j+\frac{1}{2}} := \frac{x_{j+1}+x_j}{2}\right\}_{j=0}^N$. Define the average, $v_{j+\frac{1}{2}} := \frac{v_{j+1}+v_j}{2}$ and difference operators

$$\delta_x v_{j+\frac{1}{2}} := \frac{v_{j+1}-v_j}{h}, \quad \delta_x^2 v_j := \frac{v_{j+1}-2v_j+v_{j-1}}{h^2}, \quad (23)$$

It is worth noting that by considering odd-number derivatives at the in-between nodes within the uniform discretization of $[0, L]$, higher-order approximations are achieved [12].

The ORFD approximation of equations (1) with (5) is

$$(\mathbf{C}_1 \otimes \mathbf{M}) \begin{bmatrix} \vec{v} \\ \vec{p} \end{bmatrix} + (\mathbf{C}_2 \otimes \mathbf{A}_h) \begin{bmatrix} \vec{v} \\ \vec{p} \end{bmatrix} + (\mathbf{C}_3 \otimes \mathbf{B}) \begin{bmatrix} \vec{v} \\ \vec{p} \end{bmatrix} = \vec{0}, \quad (24)$$

where C_1 and C_2 are matrices for material parameters, and C_3 is the matrix for the state feedback amplifiers, defined as

$$\mathbf{C}_1 = \begin{bmatrix} \rho & 0 \\ 0 & \mu \end{bmatrix}, \quad \mathbf{C}_2 = \begin{bmatrix} \alpha & -\gamma\beta \\ -\gamma\beta & \beta \end{bmatrix}, \quad \mathbf{C}_3 = \begin{bmatrix} \xi_1 & 0 \\ 0 & \xi_2 \end{bmatrix},$$

the $(N+1) \times (N+1)$ mass matrix \mathbf{M} is defined by

$$\mathbf{M} = \frac{1}{4} \begin{bmatrix} 2 & 1 & 0 & \dots & \dots & \dots & 0 \\ 1 & 2 & 1 & 0 & \dots & \dots & 0 \\ & \ddots & \ddots & \ddots & \ddots & \ddots & \\ 0 & \dots & \dots & 0 & 1 & 2 & 1 \\ 0 & \dots & \dots & \dots & 0 & 1 & 1 \end{bmatrix},$$

the $(N+1) \times (N+1)$ central difference matrix \mathbf{A}_h is

$$\mathbf{A}_h = \frac{1}{h^2} \begin{bmatrix} 2 & -1 & 0 & \dots & \dots & \dots & 0 \\ -1 & 2 & -1 & 0 & \dots & \dots & 0 \\ & \ddots & \ddots & \ddots & \ddots & \ddots & \\ 0 & \dots & \dots & 0 & -1 & 2 & -1 \\ 0 & \dots & \dots & \dots & 0 & -1 & 1 \end{bmatrix},$$

and the $(N+1) \times (N+1)$ boundary node matrix \mathbf{B} is a zero matrix except for the $(N+1) \times (N+1)$ -th entry, which is $\frac{1}{h}$, due to the boundary damping being injected at the last node. Here, \otimes denotes the matrix Kronecker product. It's worth noting that equation (24) can be rewritten in the first-order form as

$$\frac{d}{dt} [\vec{v} \quad \vec{p} \quad \dot{\vec{v}} \quad \dot{\vec{p}}]^T = \mathcal{A} [\vec{v} \quad \vec{p} \quad \dot{\vec{v}} \quad \dot{\vec{p}}]^T, \quad (25)$$

$$\mathcal{A} = \begin{bmatrix} \mathbf{0}_{2N+2} & \mathbf{I}_{2N+2} \\ -(\mathbf{C}_1^{-1} \mathbf{C}_2) \otimes (\mathbf{M}^{-1} \mathbf{A}_h) & -(\mathbf{C}_1^{-1} \mathbf{C}_3) \otimes (\mathbf{M}^{-1} \mathbf{B}) \end{bmatrix} \quad (26)$$

The discretized energy corresponding to (25) is

$$E_h(t) := \frac{h}{2} \left\langle (\mathbf{C}_1 \otimes \mathbf{M}) \begin{bmatrix} \dot{\vec{v}} \\ \dot{\vec{p}} \end{bmatrix}, \begin{bmatrix} \dot{\vec{v}} \\ \dot{\vec{p}} \end{bmatrix} \right\rangle + \frac{h}{2} \left\langle (\mathbf{C}_1 \otimes \mathbf{A}_h) \begin{bmatrix} \vec{v} \\ \vec{p} \end{bmatrix}, \begin{bmatrix} \vec{v} \\ \vec{p} \end{bmatrix} \right\rangle. \quad (27)$$

To show the importance of our analysis for the choices of sensor feedback amplifiers via the optimization process outlined in the previous section, sample numerical simulations are presented for the material constants in Table I.

TABLE I
Realistic Piezoelectric Material Parameters

Parameter	Symbol	Value	Unit
Length of the beam	L	1	m
Mass density	ρ	6000	kg/m ³
Magnetic permeability	μ	10^{-6}	H/m
Elastic stiffness	α	10^9	N/m ²
Piezoelectric constant	γ	10^{-3}	C/m ³
Impermissivity	β	10^{12}	m/F

Note that $\sigma_{max}(\delta)$ in (15) depends solely on the material parameters. In particular, $\sigma_{max} = \frac{1}{4\eta L} \approx 102.04$ for the material parameters in Table I. Letting $\epsilon = 1$, which is a valid choice for any system according to equations (22), the intervals for optimal sensor feedback amplifiers in (16), corresponding to σ_{max} , are as follows:

$$\begin{aligned} (c_1^-, c_1^+) &\approx (7.17 \times 10^5, 4.18 \times 10^6), \\ (c_2^-, c_2^+) &\approx (1.02 \times 10^{-4}, 9.78 \times 10^9). \end{aligned} \quad (28)$$

Here note that both the maximal decay rate $-\sigma_{max}$ and the corresponding intervals for feedback amplifiers in (28) are independent of the choice of initial conditions.

For simulations, we take $N = 80$ nodes, and we choose triangular (hat-type) initial conditions that are composed of high and low-frequency vibrational nodes. The simulations are performed for $T = 0.1$ sec to show the rapid exponential decay of solutions. Indeed, the solutions of the system (24) with the choices of optimal feedback amplifiers $\xi_1 = 10^6 \in (c_1^-, c_1^+)$ and $\xi_2 = 10^9 \in (c_2^-, c_2^+)$, are observed drive all states to zero state rapidly, e.g. see Fig. 5, and the total energy follows the exponentially decay in a higher rate than claimed σ_{max} , Fig. 7.

Our analysis indicates that even a relatively small perturbation in the values of the feedback amplifiers ξ_1 can lead to suboptimal performance. Indeed, when $\xi_1 = 10^4$ and does not fall within the range (c_1^-, c_1^+) , the system still continues to exhibit low and high-frequency longitudinal oscillations for $T = 0.1$ seconds, as demonstrated in Figure 6. Furthermore, the energy of the system decays in an unstable manner, with a decay rate significantly larger than $-\sigma_{max}$, as depicted in Figure 7.

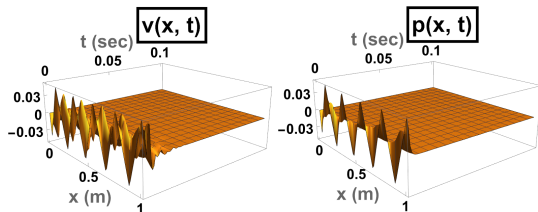


Fig. 5. System behavior for the optimal choice of feedback amplifiers: $\xi_1 = 10^6$ and $\xi_2 = 10^9$. Both solutions $v(x, t)$ and $p(x, t)$ of Equation (24) decay rapidly to the zero state in much less than 0.1 sec.

To demonstrate the robustness of our theoretical findings, we examine the spectrum of the numerical approximation. Let

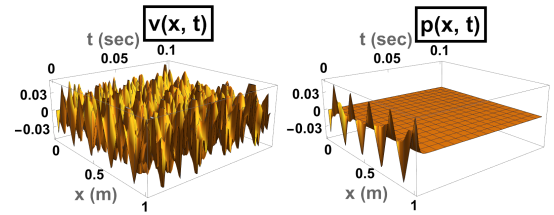


Fig. 6. For a non-optimal choice of $\xi_1 = 10^4$, which control longitudinal strains, and an optimal choice of $\xi_2 = 10^9$, controlling the voltage, the longitudinal oscillations $v(x, t)$ for eq. (24) exhibit a significantly slower decay rate.

$\xi_1 \backslash \xi_2$	10^5	$10^{5.5}$	10^6	$10^{6.5}$	10^7	$10^{7.5}$
10^{-7}	-0.1	-0.1	-0.1	-0.1	-0.1	-0.1
10^{-5}	-10	-10	-10	-10	-10	-10
10^{-3}	-17	-53	-177	-421	-101.9	-32
10^6	-17	-53	-177	-421	-101.9	-31
10^9	-17	-53	-177	-421	-101	-30
10^{10}	-17	-52	-100	-100	-97	-23
10^{11}	-10	-10	-10	-10	-10	-9

TABLE II

The $\max\{\Re(\mu_k)\}$ values for different choices of feedback amplifiers ξ_1 and ξ_2 . Red boxes indicate the intervals (c_1^-, c_1^+) and (c_2^-, c_2^+) , where the maximal decay rate is achieved.

μ_k denote the eigenvalues of \mathcal{A} as defined in Equation (26). The decay rate of the system (1) with (5), and the theoretically derived decay rate $-\sigma$ in Theorem (2), can be approximated as the maximal real part of the eigenvalues of \mathcal{A} , specifically $-\sigma \approx \max\{\Re(\mu_k)\}$. A contour plot of $\max\{\Re(\mu_k)\}$ in terms of the feedback amplifiers ξ_1 and ξ_2 is presented in Figure 8. It is notable that as the feedback amplifiers ξ_1 and ξ_2 fall within the intervals (c_1^-, c_1^+) and (c_2^-, c_2^+) , respectively shown as red lines, the maximal decay rate is achieved. Conversely, the decay rate significantly diminishes outside of these intervals. Exact values of $\max\{\Re(\mu_k)\}$ for selected feedback amplifiers are also provided in Table II. As a final note, the decay rates are much smaller than $-\sigma_{max}$ when both feedback amplifiers are chosen from the intervals (c_1^-, c_1^+) and (c_2^-, c_2^+) .

V. CONCLUSIONS & FUTURE WORK

In summary, using the Lyapunov approach, we derived the exponential decay rate “ $-\sigma$ ” for system (1), with the design of state feedback amplifiers ξ_1 and ξ_2 as described in (5). This decay rate ensures fast stabilization, though improvements are possible. The rate depends on material parameters and feedback amplifiers. Our numerical results confirm the robustness of this decay rate, with deviations affecting it from the theoretical value. Interactive simulations are available through the Wolfram Demonstrations Project [31].

A full numerical analysis and proof of exponential stability for the semi-discretized model (24), as $h \rightarrow 0$, and determining optimal designs of feedback amplifiers remain beyond this paper’s scope and are ongoing research. However, the Lyapunov approach here serves as the basis for results in [2], where the discretized model achieves the same decay rate as the PDE model.

Future work can extend these concepts to multi-layer magnetizable piezoelectric beams, which have numerous practical applications [19]. The design of feedback amplifiers may become more delicate when there are more than two state feedback amplifiers, as highlighted in [19]. There is also potential to explore general hyperbolic PDE systems with multiple boundary dampers. Relevant studies address systems with random inputs [14] and the optimal design and placement of actuators in higher-dimensional systems [15], [16], both of which are valuable for future research.

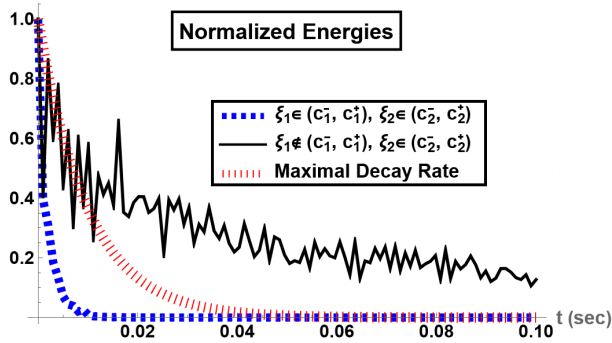


Fig. 7. Normalized total energies for (24) with optimal and non-optimal feedback amplifiers, along with the theoretically derived energy decay as stated in Theorem (3).

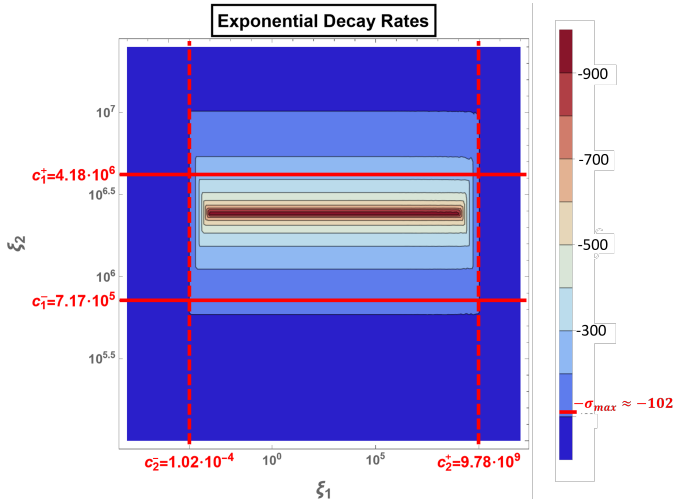


Fig. 8. Decay rates for the ORFD approximation of the system (1) with (5), showing dependence on feedback amplifiers ξ_1 and ξ_2 . Red lines mark the intervals (c_1^-, c_1^+) and (c_2^-, c_2^+) , where the maximal decay rate is achieved. Lighter blue and brown areas indicate better decay rates, while darker blue regions show slower rates outside these intervals.

[1] A. K. Aydın, A.Ö. Özer, J. Waltherman, *A Novel Finite Difference-Based Model Reduction and a Sensor Design for a Multilayer Smart Beam With Arbitrary Number of Layers*, IEEE Control Syst. Lett., 7 (2023), 1548–553.
[2] A.Ö. Özer, A.K. Aydın, J. Waltherman, *A Robust Finite-Difference Model Reduction for the Boundary Feedback Stabilization of Fully-dynamic Piezoelectric Beams*, arXiv:2309.07492, under revision, 2023.
[3] H.E. Boujaoui, H. Bouslous, L. Maniar, *Boundary Stabilization for 1-d Semi-Discrete Wave Equation by Filtering Technique* Bull. TICMI, 17-1 (2013), 1–18.

[4] N. Cîndea, A. Münch, *A mixed formulation for the direct approximation of the control of minimal L_2 -norm for linear type wave equations*, Calcolo, 52-3 (2015), 245–288.
[5] C. Dagdeviren, et al., *Recent Progress in Flexible and Stretchable Piezoelectric Devices for Mechanical Energy Harvesting, Sensing and Actuation*, Extreme Mech. Lett., 9(1) (2016), 269–281.
[6] M.C. de Jong, et al., *On control of voltage-actuated piezoelectric beam: A Krasovskii passivity-based approach*, Eur. J. Control, 69 (2023), 100724.
[7] W. Dong, et al., *Wearable human-machine interface based on PVDF piezoelectric sensor*, Trans. Inst. Meas. Control, 39-4 (2017), 398–403.
[8] I. Ftouhi, E. Zuazua, *Optimal design of sensors via geometric criteria*, J. Geom. Anal., 33-8 (2023), 253.
[9] B. Geshkovski, E. Zuazua, *Optimal actuator design via Brunovsky’s normal form*, IEEE Trans. Autom. Control, (2022) pp. 6641–6650.
[10] G.Y. Gu, et al., *Modeling and Control of Piezo-Actuated Nanopositioning Stages: A Survey*, IEEE Trans. Autom. Sci. Eng., 13-1 (2016), 313–332.
[11] J.A. Infante and E. Zuazua, *Boundary observability for the space semi-discretizations of the 1-D wave equation*, Math. Model. Num. Anal., 33 (1999), 407–438.
[12] J. Liu, B.Z. Guo, *A new semi-discretized order reduction finite difference scheme for uniform approximation of 1-D wave equation*, SIAM J. Control Optim., 58 (2020), 2256–2287.
[13] K. Kunisch, P. Trautmann, B. Vexler, *Optimal control of the undamped linear wave equation with measure valued controls*, SIAM Journal on Control and Optimization, 2016, 1212–1244.
[14] F.J. Marín, J. Martínez-Frutos, F. Periago *Robust averaged control of vibrations for the Bernoulli-Euler beam equation*. Journal of Optimization Theory and Applications. 2017, 174–428.
[15] K. Morris, M.A. Demetriou, S.D. Yang, *Using H_2 -control performance metrics for the optimal actuator location of distributed parameter systems*, IEEE Trans. Autom. Control, 60-2 (2015), 450–462.
[16] A. Münch, P. Pedregal, F. Periago, *Optimal Internal Stabilization of the Linear System of Elasticity*. Arch Rational Mech Anal 193 (2009), 171–193.
[17] K. Morris, A.Ö. Özer, *Modeling and stability of voltage-actuated piezoelectric beams with electric effect*, SIAM J. Control Optim., 52-4 (2014), 2371–2398.
[18] A.Ö. Özer, *Further stabilization and exact observability results for voltage-actuated piezoelectric beams with magnetic effects*, Math. Control Signals Syst., 27 (2015), 219–244.
[19] A.Ö. Özer, *Modeling and controlling an active constrained layered (ACL) beam actuated by two voltage sources with/without magnetic effects*, IEEE Trans. Autom. Control, 62-12 (2017), 6445–6450.
[20] A.Ö. Özer, K.A. Morris, *Modeling and related results for current-actuated piezoelectric beams by including magnetic effects*, ESAIM: COCV, 26-8 (2019), 1–24.
[21] A.Ö. Özer, W. Horner, *Uniform boundary observability of Finite Difference approximations of non-compactly-coupled piezoelectric beam equations*, Appl. Anal., 101-5 (2022), 1571–1592.
[22] Y. Privat, E. Trélat, E. Zuazua, *Actuator design for parabolic distributed parameter systems with the moment method*, SIAM J. Control Optim., 55-2 (2017), 1128–1152.
[23] A.J.A. Ramos, M.M. Freitas, D.S. Almeida Jr., S.S. Jesus, T.R.S. Moura, *Equivalence between exponential stabilization and boundary observability for piezoelectric beams with magnetic effect*, Z. Angew. Math. Phys., 70-60 (2019).
[24] *Ultrasound imaging of the brain and liver*, Science Daily, Acoust. Soc. Am., 26 June 2017.
[25] Q. Shi, T. Wang, C. Lee, *MEMS Based Broadband Piezoelectric Ultrasonic Energy Harvester (PUEH) for Enabling Self-Powered Implantable Biomedical Devices*, Sci. Rep., 6 (2016), 24946.
[26] R.C. Smith, *Smart Material Systems*, (SIAM, 2005).
[27] T. Voss, J.M.A. Scherpen, *Stabilization and shape control of a 1D piezoelectric Timoshenko beam*, Automatica, 47-12 (2011), 2780–85.
[28] J. Yang, *An Introduction to the Theory of Piezoelectricity*, Springer, New York, 2005.
[29] B. Yubo, C. Prieur, Z. Wang, *Stabilization of a Rayleigh beam with collocated piezoelectric sensor/actuator*. Evol. Equ. Control Theory, (2023).
[30] L.T. Tebou, E. Zuazua, *Uniform boundary stabilization of the finite difference space discretization of the 1-D wave equation*. Adv. Comput. Math., 26 (2007), 337–365.
[31] J. Waltherman, A.K. Aydın, A.Ö. Özer, *Piezoelectric beam dynamics*, Wolfram Demonstrations Project, Published: June 13, 2023.
[32] H.S. Wang, et al., *Biomimetic and flexible piezoelectric mobile acoustic sensors with multiresonant ultrathin structures for machine learning biometrics*, Sci. Adv., 7-7 (2021).